Korean J. Chem. Eng., 35(4), 984-993 (2018)
DOI: 10.1007/s11814-017-0347-z

pISSN: 0256-1115
eISSN: 1975-7220

Agomelatine co-crystals with resorcinol and hydroquinone: Preparation and characterization

Min-Jeong Lee*, Nan-Hee Chun, Hyo-Cheol Kim***, Moon-Jip Kim***, Paul Kim****, Min-Yong Cho****, and Guang Jin Choi****,*****,†**

*Crystallization and Particle Science, Institute of Chemical and Engineering Sciences, A*STAR (Agency for Science, Technology and Research), 1 Pesek Road, Jurong Island 627833, Singapore
**Unimed Pharm Inc., Asan, Chungnam 31501, Korea
***Department of Physics, Soonchunhyang University, Asan, Chungnam 31538, Korea
****Department of Pharmaceutical Engineering, Soonchunhyang University, Asan, Chungnam 31538, Korea
*****Department of Medical Science, Soonchunhyang University, Asan, Chungnam 31538, Korea
(*Received 16 October 2017 • accepted 12 December 2017*)

Abstract−We prepared and characterized co-crystals of the antidepressant drug agomelatine with pharmaceutically acceptable coformers for enhanced solubility. A novel agomelatine-resorcinol (AGO-RES, 2 : 1) co-crystal was synthesized and its crystal structure was confirmed via single crystal X-ray diffraction. The AGO-RES co-crystal structure was created through the O-H···O and N-H···O hydrogen bonding between the phenolic OH of RES and the amide group of AGO. The chemical structure of two AGO co-crystals was characterized by FT-IR and Raman spectroscopies, whereas the solution behavior was determined by the intrinsic dissolution rate. When tested in water, both AGO-RES and AGO-HYQ form-I co-crystals showed higher apparent solubility than pure AGO. But the resulting AGO solution in a supersaturated state partially precipitated into specific crystal forms of AGO. As anticipated, the intrinsic dissolution rate of AGO was substantially enhanced by the co-crystal forms, which signifies that the bioavailability of AGO can be increased via co-crystal formulation approach.

Keywords: Co-crystal, Agomelatine, Resorcinol, Hydroquinone, Solubility

INTRODUCTION

Pharmaceutical co-crystals are stoichiometric molecular complexes that contain active pharmaceutical ingredients (APIs) and pharmaceutically acceptable coformers in a crystal lattice via non-covalent interactions, predominantly hydrogen bonds [2-4]. In 2016 [5], the FDA reclassified the pharmaceutical co-crystals as a special case of solvates and hydrates where the second component, the coformer, is nonvolatile, modifying their earlier viewpoint as a drug product intermediate (DPI) or as an in-process material in 2013 [6]. In the 2016 guidance, the FDA describes: "co-crystals can be tailored to enhance drug product bioavailability and stability and to enhance the processability of APIs during drug product manufacture."

The coformers are usually selected from the generally regarded as safe [7] and/or everything added to food in the United States [8] lists of the US FDA. A number of pharmaceutical co-crystals have been reported to modify physicochemical properties of APIs, such as solubility, dissolution rate, hygroscopicity and stability [4,9-12]. Up to now, various methods and processes have been developed to enable the potential of the co-crystal approach [13].

Agomelatine (AGO, Fig. 1) is an anti-depressant drug with a melatonergic agonist and complementary 5-hydroxytryptamine 2C (5-HT2C) antagonist properties [14]. It is used to treat major depressive disorders and is marketed as Valdoxan or Thymanax in Europe [15]. AGO has poor water solubility (<0.1 mg/mL) [16], prompting investigation into polymorphs and solvates of AGO to improve solubility [17]. Six polymorphic forms of AGO have been reported to date, designated as forms I-VI [18].

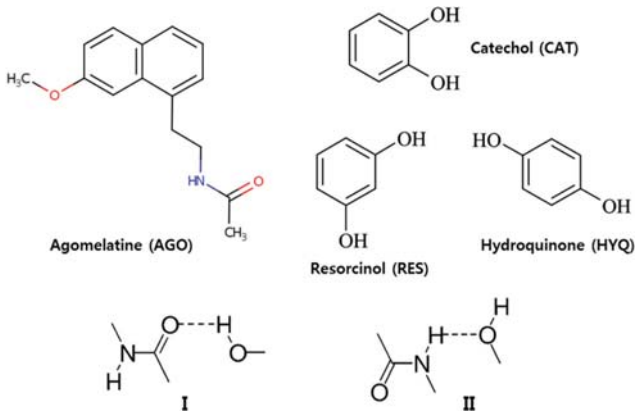

Fig. 1. Chemical structures of agomelatine (AGO) and phenolic coformers (top). Possible hydrogen bonding synthons between amide and hydroxyl groups (bottom).

The present study was inspired by a recent article reporting ago-

†To whom correspondence should be addressed.
E-mail: guangchoi@sch.ac.kr

melatine co-crystals with urea, glycolic acid, isonicotinamide, and methyl 4-hydroxybenzoate [19]. The authors presented potential hydrogen bonding relationships between synthons containing the 2° amide group of agomelatine with various functional groups based upon the Cambridge Structural Database (CSD) survey. About 12% of crystal structures that contain at least one 2° amide group exhibit heterosynthons I and II (Fig. 1) [19], noting that none of these coformers contained hydroxyl groups in their structure.

Therefore, we chose phenolic compounds as coformer in the design and construction of agomelatine co-crystals. Catechol (CAT), resorcinol (RES), and hydroquinone (HYQ) are dihydroxybenzene isomers widely used in cosmetic, medicine, pesticides, flavoring agents, and dyes [20]. The primary difference between them is the position of hydroxyl groups bonded to their structural benzene ring, which could lead to the formation of co-crystals with different properties (Fig. 1). In the middle of our exploration with two novel AGO co-crystals with RES and HYQ, another team [1] reported crystal structures of two polymorphic AGO co-crystals with HYQ based on X-ray measurements.

We report here the synthesis of a novel AGO-RES co-crystal and its characterization using the powder X-ray diffraction and single-crystal X-ray diffraction, differential scanning calorimetry (DSC), thermogravimetric analysis (TGA), Fourier transform infrared (FTIR) spectroscopy and Raman spectroscopy. In addition, AGO-HYQ form I co-crystal was prepared by solvent evaporation method and characterized for comparison with previous reported data. Solubility and dissolution behaviors of several co-crystal materials were investigated for correlation with analytical data.

MATERIALS AND METHODS

Various dihydroxybenzene isomers used as coformer have two polar functional groups which can be involved in the formation of hydrogen bonding with an amide group of agomelatine (AGO) toward supermolecular co-crystal structure, as shown in Fig. 1. During the grinding screening, two molar ratios were examined: 1 : 1 and 2 : 1 (drug/coformer).

1. Materials

AGO form II (purity ≥99.85%, Changzhou R. Pharm. Co., Changzhou, China) was used without further purification. Catechol (CAT), hydroquinone (HYQ) and resorcinol (RES) were purchased from Sigma Aldrich Co. (St. Louis, MO, USA). These coformers were used as supplied. All other chemicals including organic solvents were supplied by Merck (New York, USA).

When cathechol (CAT) was ground as coformer with AGO, the mixture was melted during grinding. Accordingly, no apparent solid product was obtained for AGO-CAT combinations. It seems that a eutectic was produced, instead.

2. AGO Co-crystal Preparation by Grinding

The solid state grinding was performed in two ways: neat grinding (NG) and liquid-assisted grinding (LAG). All grinding work was carried out manually using a mortar and pestle. For NG, a mixture of agomelatine (122 mg, 0.5 mmol) and each coformer in a designated molar ratio was mixed and ground for 20 min. On the other hand, a few drops of a specific solvent were added for LAG prior to grinding for 20 min. Among common organic solvents, selected were methanol, ethanol, acetone, and ethyl acetate. Whether AGO co-crystals were created was determined based on PXRD and DSC data, by comparing the PXRD patterns and DSC thermograms for resulting powders with those for starting materials.

3. Ago Co-crystal Preparation by Solvent Evaporation

For AGO-RES co-crystal, 2 : 1 mixture of AGO (973 mg, 4 mmol) and RES (220 mg, 2 mmol) was dissolved in 100 mL of ethyl acetate. The solution was left open in a container at room temperature until fully evaporated. Usually it took a full day. For AGO-HYQ co-crystal, 1 : 1 mixture of AGO (973 mg, 4 mmol) and HYQ (440 mg, 4 mmol) was dissolved in 100 mL of ethyl acetate. The solution was treated exactly the same as the AGO-RES combination. After the evaporation was complete, the remnant solid was collected and dried overnight under vacuum, followed by various characterization procedures.

The powder specimen for the single crystal X-ray diffraction (SC-XRD) was obtained by vapor diffusion method. Co-crystal powders prepared by solvent evaporation were used as raw material for growing single crystals of a sufficient size by the vapor diffusion experiment. AGO-RES co-crystal of 100 mg was dissolved in 2 mL of ethyl acetate in a 5 mL vial. Then, the vial with slightly opened cap was placed in a chamber containing 10 mL of hexane. Approximately after four days, colorless clear crystals were obtained. An optical microscope was used to pick the best quality crystal powder for SC-XRD measurements.

4. Powder X-ray Diffraction (PXRD)

PXRD data were recorded on a MiniFlex 600 X-ray diffractometer (Rigaku, Tokyo, Japan) using a Cu-Kα radiation source (λ= 1.5406 Å) at 40 kV and 15 mA. Diffraction patterns were collected over a 2θ range of 5-30° with a step size of 0.02° and a scan rate of 10°/min. D/teX ultra-detector with greater intensity measurement capability was used for higher resolution.

5. Single Crystal X-ray Diffraction (SC-XRD)

X-ray reflections were collected on a diffractometer (Enraf-Nonius CAD-4, Delft, Holland) diffractometer with graphite mono-chromated Cu-Kα radiation (λ=1.54178 Å). The crystal powder specimen was placed on a fiber needle, and then mounted on the goniometer of the X-ray diffractometer. Data were collected and processed using CAD-4 PC (Enraf-Nonius) software. Structure was solved by direct methods and SHELXL was used for least-squares refinement.

6. Thermal Analysis

Differential scanning calorimetry (DSC) was performed using a DSC-60 instrument (Shimadzu, Kyoto, Japan). Samples (3-5 mg) were loaded in an aluminum pan (with a blank pan as reference) and scanned from 30 to 200 °C at a heating rate of 10 °C/min under a nitrogen atmosphere (flow rate: 50 mL/min).

The weight loss of samples as a function of temperature was measured using a TGA Q50 (TA Instruments, New Castle, DE, USA). Specifically, approximately 10 mg of sample was placed in the sample pan and heated over a range of 25-350 °C at a heating rate of 10 °C/min with a nitrogen purge.

7. Vibrational Spectroscopy

IR spectra were obtained with a Nicolet iS10 FTIR spectrometer (Thermo Scientific, MA, USA), equipped with a smart iTR-attenuated total reflection (ATR) accessory with a ZnSe crystal. FTIR

spectra were recorded in transmittance mode at a resolution of 4 cm^{-1} over a wavenumber range of 4,000-650 cm^{-1}.

Raman spectra were obtained using an InVia Raman microscope (Renishaw Plc, Gloucestershire, UK) with a 785-nm laser source. Spectra were collected in extended scan mode over a range of 3,200-100 cm^{-1}.

8. Solubility and Intrinsic Dissolution Rate (IDR)

Solubility was determined by using the shake-flask method, by stirring an excess amount of solid powder (AGO, AGO-RES and AGO-HYQ) into water at 37 °C for 24 h. Samples were withdrawn at predetermined time intervals and filtered with 0.45-μm nylon filters. The concentration of AGO was measured by ultraviolet (UV) spectroscopy; absorbance was measured at 328 nm to avoid interference. Calibration plots were constructed through a concentration range of 2-50 μg/mL (R^2=0.99, n=5) prior to solubility and dissolution experiments.

Intrinsic dissolution rate (IDR) experiments were conducted with a Distek 2100 dissolution apparatus, equipped with a heater/circulator. Each compound (AGO=50 mg, AGO-RES=~61 mg, and AGO-HYQ=~73 mg) was compressed in a stainless steel die using a hydraulic press (Specac Ltd., MO, USA) to form drug pellets (d= 13 mm). PXRD analysis confirmed that no phase change occurred during pellet preparation. Only one side of the drug pellet was exposed to a solution of 900 mL of phosphate buffer (pH=6.8) and 0.1 M HCl (pH=1.2) in a jar, which was preheated to 37 °C and stirred at 50 rpm. At regular time intervals, 2 mL of the sample was withdrawn, filtered using a 0.45-μm nylon filter, and analyzed for AGO concentrations using UV spectroscopy.

9. High Pressure Liquid Chromatography (HPLC)

Solute composition during dissolution experiment was determined by high pressure liquid chromatography (HPLC). Designated amount of individual components was dissolved in methanol and analyzed for concentration calibration. An Agilent 1100 series HPLC (Agilent Technologies, CA, USA) with a diode array detector and a ZORBAX eclipse plus C18 column (Agilent, 4.6×150 mm, 3.5 μm) were used. The HPLC analysis was at room temperature with a flow rate of 1 mL/min, and the mobile phase was a mixture of methanol and ultrapure water (80 : 20% (v/v)). The volume of the injected samples was 5 μL and AGO content was assayed at 230 nm. A calibration curve was constructed using standards of 0.005-0.05 mg/mL in methanol.

RESULTS AND DISCUSSION

1. AGO-RES Co-crystal Structure by SC-XRD Measurements

Single crystal X-ray diffraction analysis confirmed co-crystal formation and a 2 : 1 stoichiometry of the individual components. AGO-RES co-crystal molecules crystallized in the monoclinic $P2_1/c$ space group with two molecules of AGO and one molecule of RES in the asymmetric unit (Table 1 and Fig. 2). The amide group of AGO interacts with the phenolic O-H groups of RES to form N-H···O [N1′-H1′···O4, 2.218 Å, 2.987(4) Å, 147.85°] and O-H···O [O3-H3···O2′, 1.86(4) Å, 2.736(3) Å, 173.55°] hydrogen bonds (Table 2). These interactions propagate along the b-axis and form zigzag chains (Fig. 2). In addition to this interaction, one phenolic O-H group of RES forms O-H···O [O4-H4···O2, 1.72(3) Å, 2.637(3) Å, 174.93°] hydrogen bond to the amide C=O group of the second AGO molecule. Overall, the adjacent layers in the crystal structure pack in antiparallel fashion and the interlayer regions are dominated by weak van der Waals interactions. The diffraction patterns of AGO-RES co-crystal obtained by solvent evaporation matched the calculated diffraction patterns from the single crystal structure.

Table 1. Crystallographic data for AGO-RES Co-crystal

	AGO-RES
Chemical formula	$C_{36}H_{40}N_2O_6$
Formula weight	596.70
Crystal system	Monoclinic
Space group	$P2_1/c$
T (K)	298(2)
a (Å)	12.0312(5)
b (Å)	21.0836(10)
c (Å)	12.8392(7)
α (°)	90.00
β (°)	99.575(4)
γ (°)	90.00
V (Å^3)	3211.4(3)
D_{calc} (g cm^{-3})	1.2342
μ (mm^{-1})	0.6767
θ range	3.73-67.43
Z	4
R_1, wR_2 [$I>2\sigma(I)$]	0.0674, 0.1751
R_1, wR_2 [all data]	0.0863, 0.1910
GOF	1.046

2. AGO-RES Co-crystal by Grinding

There are many cases where eutectic products result instead of the anticipated co-crystal materials. In terms of PXRD patterns, co-crystals should be clearly different from individual components caused by hydrogen bonds and intermolecular interactions, whereas eutectics would appear very similar to starting constituents.

In our AGO-RES case, there was a clear differentiation in PXRD patterns because strong diffraction peaks from AGO and RES powders were not detected for the AGO-RES pair. Thus, produced were ARI-ORC co-crystals, not eutectic materials. It might be necessary to investigate further the AGO-CAT pair because eutectics can confer dual advantages of solubility (because of high thermodynamic functions) and stability (due to their crystalline nature) as bioavailable drug forms [21].

PXRD analysis was the primary tool used to identify new co-crystals by differentiating the co-crystal forms either from physical mixtures of the AGO and coformers or from eutectic products. Fig. 3(a) shows a typical PXRD pattern of the AGO-RES combination obtained by NG. Characteristic peaks for AGO-RES co-crystals were observed at 2θ=7.25, 7.95, 8.35 and 14.45°. Accordingly, it is obvious that there is a distinct difference between the products and the starting materials.

Fig. 3(b) illustrates typical DSC thermograms of AGO-RES powders obtained by NG, which presents two endotherms (at approximately 60 °C and 85 °C) that are different from the melting peaks

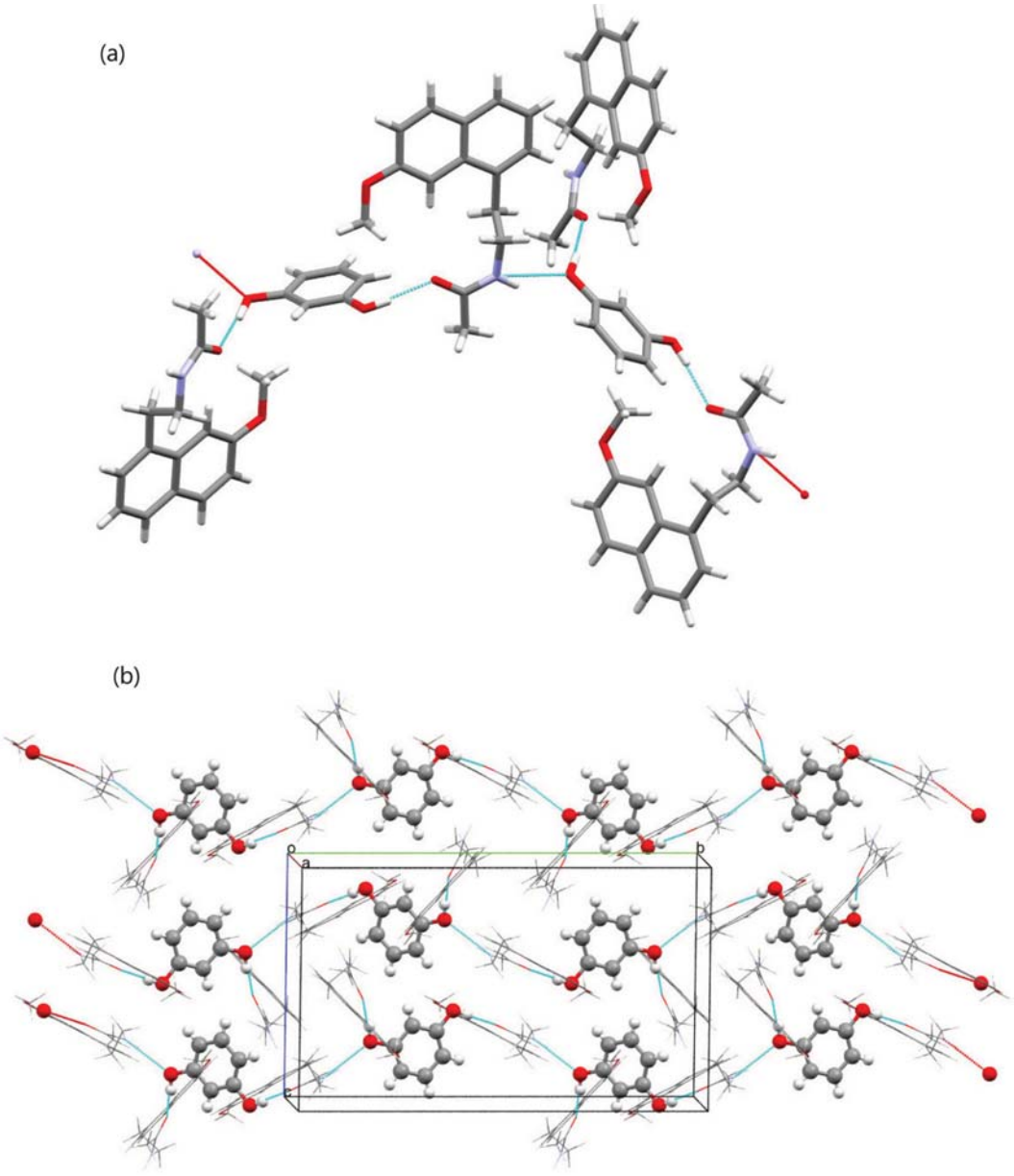

Fig. 2. (a) Crystal structure of AGO-RES co-crystal showing the interactions between AGO and RES molecules. (b) Packing diagram of AGO-RES co-crystal. The AGO molecules were drawn with wireframe model while RES molecules were highlighted as ball and stick model.

Table 2. Hydrogen-bond geometries for AGO-RES co-crystal

D-H···A	H···A (Å)	D···A (Å)	∠D-H···A (°)
N1′-H1′···O4[a]	2.218	2.987(4)	147.85
O3-H3···O2′	1.86(4)	2.736(3)	173.55
O4-H4···O2[b]	1.72(3)	2.637(3)	174.93

[a]−x+1, +y+1/2, −z−1/2
[b]x−1, −y+1/2, +z−1/2.

of the individual components (AGO=109 °C and RES=110 °C). For RES, there is a shoulder peak right in front of the main melting peak. A similar DSC peak shape was found in an article [22]. Since all coformer powders used in this study were of high purity (≥99.0%), the small peak for RES is not likely to be associated with impurity.

It has been reported that a binary drug-coformer mixture capable of forming co-crystal results in two invariant endotherms in DSC curves, where these endotherms can be attributed to eutectic and co-crystal melting [23-26]. To examine this premise, physical mixtures of AGO and RES were compounded for NG at two molar ratios (1 : 1 and 2 : 1) and analyzed via DSC at a heating rate of 5 °C/min.

Fig. 3(c) shows that there are two invariant temperatures in the DSC thermogram, indicating endotherms at 60 °C and 85 °C. By comparing this with DSC data for ground AGO-RES (Fig. 2(b)), it

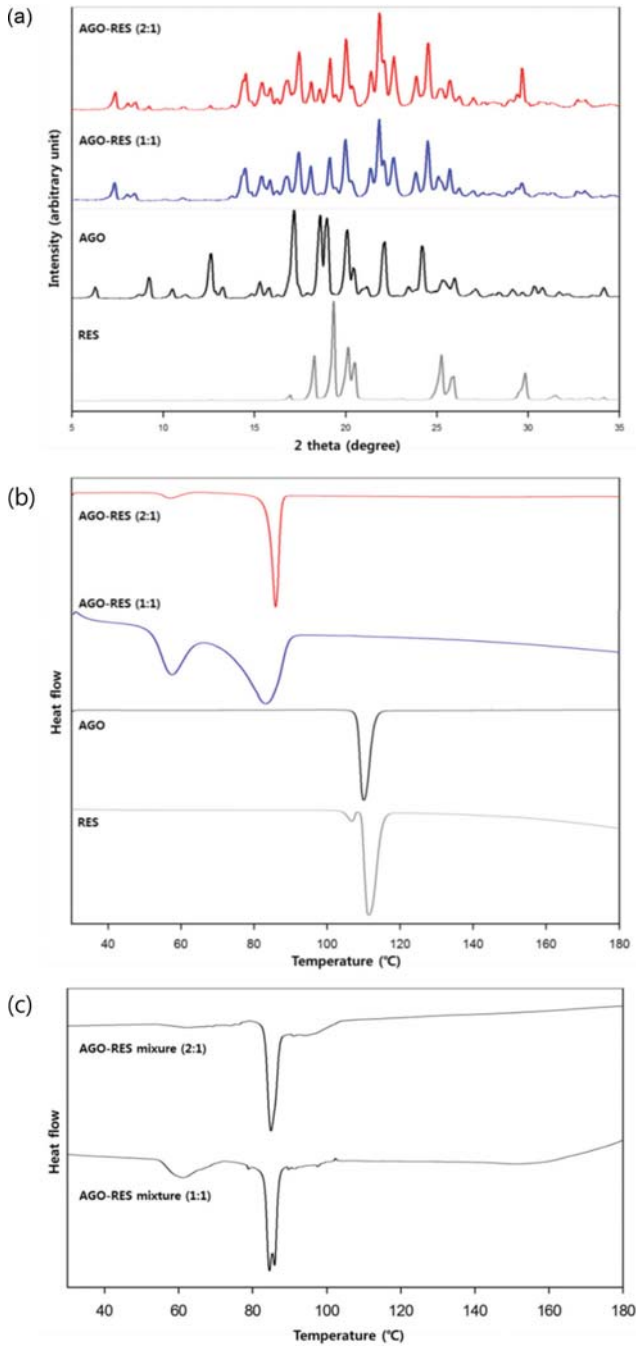

Fig. 3. (a) PXRD patterns and (b) DSC thermograms of AGO, RES and AGO-RES grinding products, and (C) DSC thermograms of AGO-RES 1 : 1 and 2 : 1 mixture powders.

could be speculated that the first endotherm is attributed to eutectic melting of unreacted AGO-RES, whereas the second is to the melting of AGO-RES co-crystal. This indicates that the formation of AGO-RES co-crystals by NG is eutectic-mediated co-crystallization [27,28]. The conversion to pure co-crystal phases was not fully achieved merely by NG or LAG alone.

3. AGO-RES and AGO-HYQ Co-crystals by Solvent Evaporation

Fig. 4 summarizes the results of the ARI-RES combination with

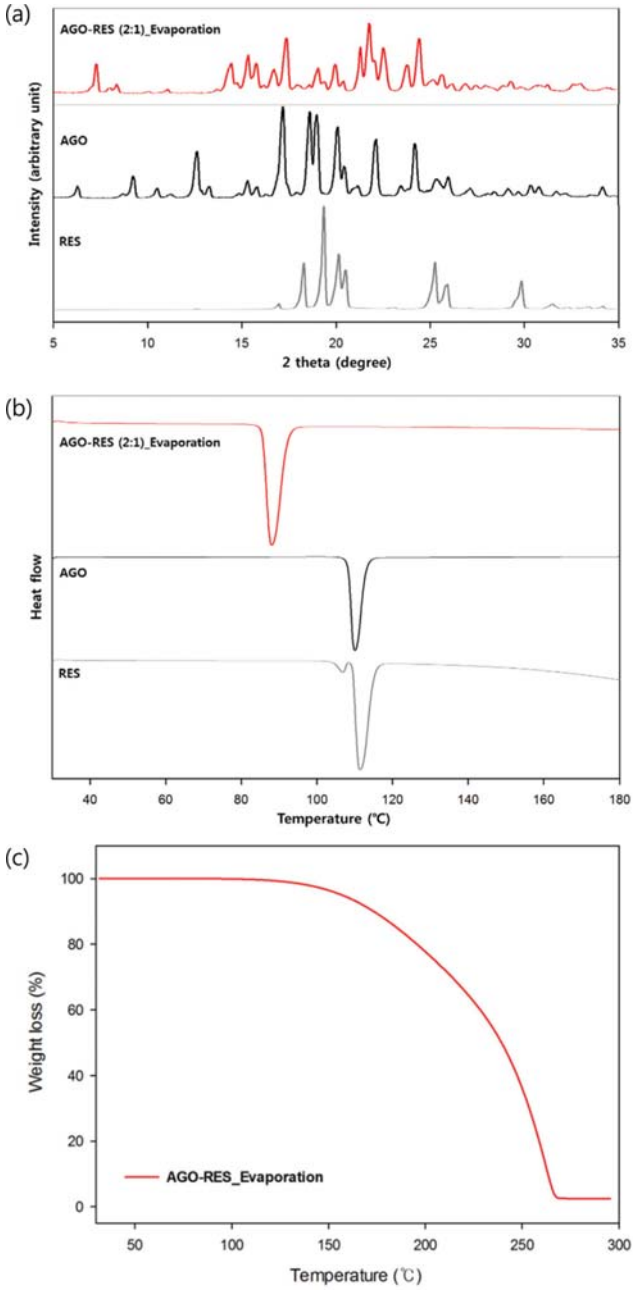

Fig. 4. (a) PXRD patterns, (b) DSC thermograms, and (c) TGA profiles of AGO-RES (2 : 1) co-crystal prepared by solvent evaporation.

2 : 1 molar ratio by solvent evaporation. The PXRD pattern (Fig. 4(a)) of the solid product shows that AGO-RES co-crystal was generated. This was further confirmed by DSC analysis (Fig. 4(b)), which gives a single sharp endothermic peak at 87 °C attributed to AGO-RES co-crystal melting. TGA profile (Fig. 4(c)) presents there was no weight loss corresponding to solvent loss. Meanwhile, the DSC curve of the evaporation product at a 1 : 1 molar ratio shows two endotherms, similar to products obtained by grinding (not shown). Therefore, 2 : 1 is a more suitable stoichiometric ratio than 1 : 1 for the AGO-RES co-crystal. It was also confirmed by the composition analysis of the pure AGO-RES co-crystal powder using

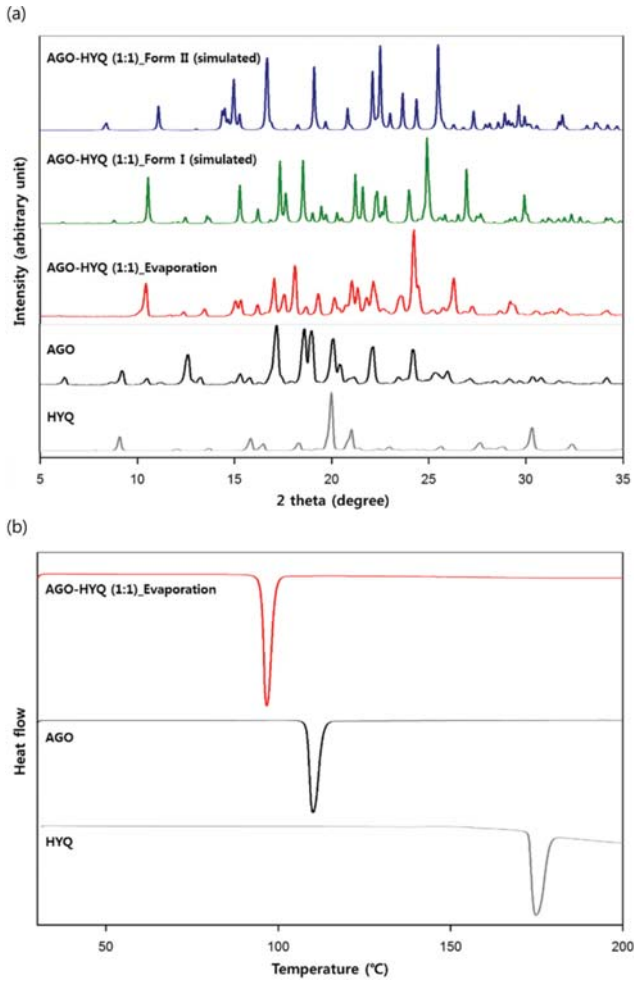

Fig. 5. (a) PXRD patterns and (b) DSC thermogram results of AGO-HYQ (1 : 1) co-crystal prepared by solvent evaporation.

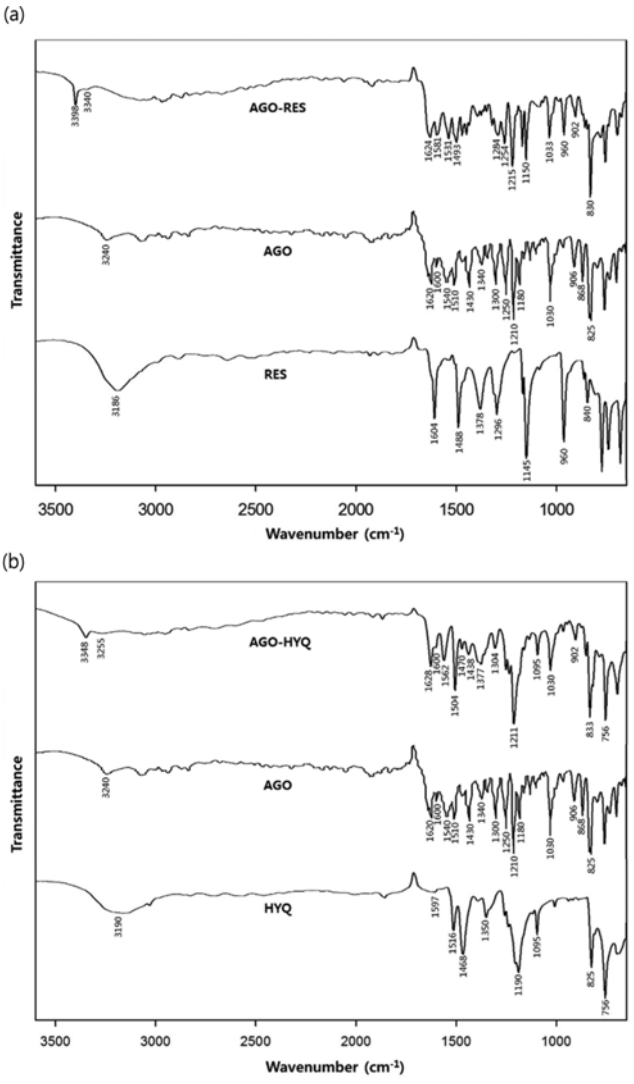

Fig. 6. FTIR spectra of (a) AGO-RES and (b) AGO-HYQ co-crystals.

HPLC. Since the AGO content in the co-crystal powder was 80.55± 0.28 (%), the molar ratio of AGO and RES was proved to be 2 : 1.

AGO-HYQ co-crystal was also prepared by solvent evaporation. Fig. 5(a) compares the PXRD patterns of the various materials. Although there is a slight down-shift in XRD peak positions, the XRD pattern of our AGO-HYQ co-crystal powders is very similar to form I among two polymorphs reported in the literature [1]. Since peaks at higher Bragg angles gave a larger shift compared to those at lower 2θ values, this peak shift would be primarily due to the lattice expansion. The HPLC analysis showed the percentage of AGO was 69.03±0.36% by weight, and it coincides with the theoretical percentage of 68.05% AGO for the 1 : 1 stoichiometry between AGO and HYQ. TGA result signifies that there is no residual solvent in the crystal prepared by solvent evaporation.

Fig. 5(b) shows DSC thermograms of AGO-HYQ combination powder prepared by solvent evaporation in comparison with the AGO and HYQ powders. Two polymorphs have been known for AGO-HYQ co-crystal by a previous study [1] based on two DSC melting points at 81 °C (form I) and 93 °C (form II). In this study, however, we observed a sharp endotherm at 95 °C (onset) clearly different from the above two. According to the literature [1], AGO-HYQ form I and form II co-crystals are monotropically related. This means that form II is thermodynamically more stable than form I at all temperatures below the melting point of form II. However, it could be changed if the melting point of form I is not 81 °C. Therefore, further experiments would be necessary to figure out the thermodynamic relationship between AGO-HYQ co-crystals form I and form II because understanding the thermodynamic relationships in co-crystal polymorphs is crucial for subsequent production of the desired polymorph in bulk [29-31].

4. Spectroscopic Analysis

FTIR spectroscopy has been widely used as a technique that can provide evidences of co-crystal formation [32]. Overlaid FTIR spectra of AGO, RES, and AGO-RES are illustrated in Fig. 6(a). AGO shows characteristic absorption peaks at 1,620 and 3,240 cm^{-1}, which can be assigned to C=O and N-H stretching of the secondary amide, respectively. The RES spectrum shows a broad peak corresponding to phenolic O-H stretching at 3,186 cm^{-1}. The N-H stretching frequency of AGO and the phenolic O-H stretching frequency of RES dramatically shift to higher wavenumbers

Table 3. Infrared characteristics of AGO, RES, HYQ, and associated co-crystals

Wavenumber (cm^{-1})					Peak assignment (Mayo et al., 2004; Socrates, 2001)
AGO	RES	HYQ	AGO-RES	AGO-HYQ	
3240			3398	3348	N-H stretching
	3186	3190	3340	3255	O-H stretching
1620			1624	1628	C=O stretching
1600	1604	1516	1581	1600	Aromatic C=C stretching
1540			1531	1562	N-H bending (amide II)
1250	1296	1190	1284	1211	C-O stretching

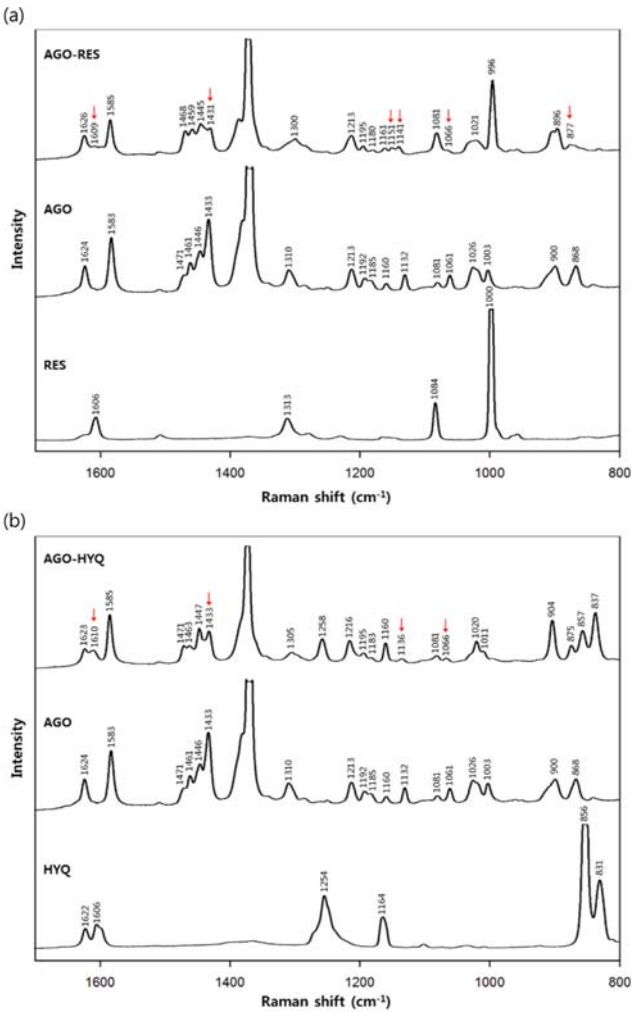

Fig. 7. Raman spectra of (a) AGO-RES and (b) AGO-HYQ co-crystals.

(3,398 and 3,340 cm^{-1}, respectively) for the AGO-RES co-crystal. These blue shifts suggest the formation of new supramolecular synthons during co-crystallization. The C=O stretching frequency of the AGO also shifted to 1,624 cm^{-1}, indicating that the C=O group participates in hydrogen bonding when the co-crystal is formed. Such a change can also be observed in the AGO-HYQ co-crystal system (Fig. 6(b)). The O-H stretching frequency of HYQ and the AGO N-H stretching frequency are shifted to 3,348 and 3,255 cm^{-1} for the co-crystal. Spectral changes associated with other functional groups in addition to N-H and O-H groups are summarized in Table 3. These results suggest that the molecular complex of AGO-HYQ exists as a co-crystal form.

Raman spectroscopy was also employed to identify co-crystallization, as its high capability to provide a molecular fingerprint has been well known [33]. Fig. 7(a) and (b) show the Raman spectra of AGO-RES, AGO-HYQ, and starting materials over the 1,700-800 cm^{-1} region, where representative vibrational wavenumbers and assignments are listed in Table 4. Spectral peak positions of AGO-RES were different when compared with AGO and RES, providing definitive evidence for co-crystal formation. The main peaks of AGO are associated with amide I C=O stretching at 1,624 cm^{-1} and aromatic ring C=C stretching at 1,583 cm^{-1}. Peaks in the 1,490-1,340 cm^{-1} region are usually assigned to the CH_2 and CH_3 deformation, whereas other peaks in the 1,340 to 1,050 cm^{-1} spectral region are assigned to the amide III band (C-N stretching, C-N bending, and N-H bending), as well as C-O stretching, C-C stretching and various bending vibrations [34,35].

The Raman spectrum of RES has characteristic bands at 1,606, 1,311 and 1,084 cm^{-1}, where the first may be attributed to C=C stretching within the aromatic ring, and two other bands to C-O stretching vibration of the hydroxyl group. Formation of the AGO-RES co-crystal causes AGO and RES Raman bands to shift with an overall decrease in intensity. This is especially true for the peak

Table 4. Characteristic raman peaks of AGO, RES, HYQ, and associated co-crystals

Wavenumber (cm^{-1})					Peak assignment (Mayo et al., 2004; Socrates, 2001)
AGO	RES	HYQ	AGO-RES	AGO-HYQ	
1624			1626	1623	C=O stretching
1583	1606	1606	1585	1585	C=C stretching
1310			1300 (broad)	1305 (broad)	Amide III band (C-N stretching, N-H bending)
1212	1084	1254	1081	1258	C-O stretching

at 1,606 cm^{-1} in the RES spectrum and bands observed at 1,433, 1,132, 1,061 and 868 cm^{-1} in the AGO spectrum, all of which decrease greatly in the AGO-RES co-crystal spectrum. In addition to these changes, a new peak at 1,151 cm^{-1} was observed in the AGO-RES co-crystal spectrum, which was not detected in either AGO or RES spectra.

Characteristic bands at 1,606, 1,254 and 1,164 cm^{-1} were observed from the Raman spectrum of HYQ. The first band may be assigned C=C stretching vibrations from the aromatic ring while the others would be attributed to C-O stretching vibrations of the hydroxyl group. These bands shift to 1,610, 1,258, and 1,160 cm^{-1} in the AGO-HYQ co-crystal spectra. Although there are no new peaks in the Raman spectrum of AGO-HYQ, the bands of AGO and HYQ are shifted and the intensity reduced upon co-crystallization similar as the AGO-RES co-crystal. Analysis of Raman spectra thus confirms that there is significant alteration in intermolecular interactions (specifically hydrogen bonding) upon co-crystal formation.

5. Solubility and Intrinsic Dissolution Rate (IDR)

AGO is one of the insoluble drug substances (<0.1 mg/mL in water) whereas the RES and HYQ are much more soluble in aqueous media (RES=1,100 mg/mL; HYQ=70 mg/mL). To measure solubility, excess powder samples of AGO-RES and AGO-HYQ co-crystal powders were suspended in purified water and stirred at 37 °C for 24 h. Each testing solution was sampled at designated time intervals and diluted prior to determining the AGO concentrations using UV spectroscopy. The resulting solubility profiles are illustrated in Fig. 8. Peak AGO concentration values for both AGO-RES and AGO-HYQ co-crystal powders were reached at 30 and 90 min, respectively. On the other hand, the AGO concentrations of AGO-RES and AGO-HYQ combinations measured after 24 h were approximately 2.5 and 3.5 times greater, respectively, than that of the pure AGO powder specimen.

Fig. 9 illustrates the results of PXRD analysis on the solids remaining after solubility experiments. For the AGO-RES co-crystal, AGO dissolved from the co-crystal was partly precipitated to create the AGO form I, while supersaturated AGO from the AGO-HYQ co-crystal was solidified to a mixture of co-crystal and AGO form III.

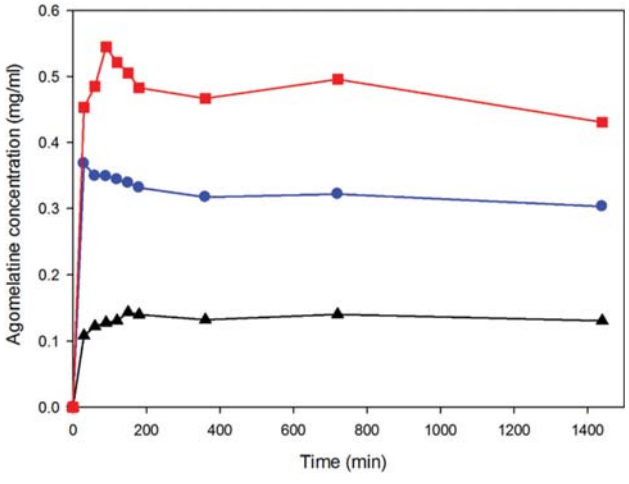

Fig. 8. Solubility profiles of AGO (▲), AGO-RES (●), and AGO-HYQ (■).

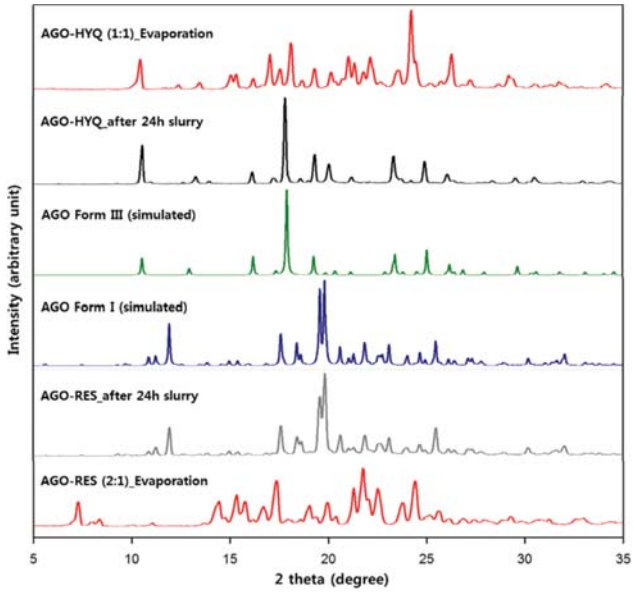

Fig. 9. PXRD patterns of precipitates after solubility analysis of AGO-RES and AGO-HYQ co-crystals.

Although PXRD results indicate that both AGO-RES and AGO-HYQ are not indefinitely stable in water, the concentration of AGO plateaus until 24 h. This supports the "spring and parachute" effect of co-crystals, which can be described as follows: the dissociation of the co-crystal into an amorphous-like drug form, the generation of a metastable form, and maintenance of a high drug concentration over an extended time [3].

In many cases, the solubility of co-crystals is highly proportional to the solubility of its coformer compounds [36]. Hence, a novel co-crystal with a higher solubility could be anticipated by incorporating coformer molecules with greater aqueous solubility into the superlattice structure. The solubility of RES is much higher than that of HYQ, whereas the solubility of AGO-RES is lower than the solubility of AGO-HYQ. A possible cause for this solubility discrepancy between the expected and measured values could be the pH values of suspensions. The pH value of AGO suspension after solubility experiment was 5.46, while the pH values of aqueous suspensions of AGO-RES and AGO-HYQ were 5.09 and 4.25, respectively. These values were not significantly different from the pH values of RES aqueous solution (5.08) and HYQ aqueous solution (4.31). Considering the pKa of AGO (15.96) [37], it is readily anticipated that the solubility of AGO-HYQ is higher than the solubility of AGO-RES. This might also have influenced the transformation of different metastable forms in the "parachute" stage. As shown in Fig. 9, AGO-RES and AGO-HYQ co-crystals were mostly converted to AGO forms I and III, in which the AGO form I has a lower reported solubility than form III in aqueous solutions [38].

For intrinsic dissolution rate (IDR) measurements, powder samples were compressed into a 1.33 cm^2 pellet for a fixed surface area and exposed to two types of dissolution media, the phosphate buffer (pH 6.8) and hydrochloric acid buffer (pH 1.2). Sample solutions were collected at designated time intervals to measure the AGO concentrations using calibrated UV spectroscopy. IDR pro-

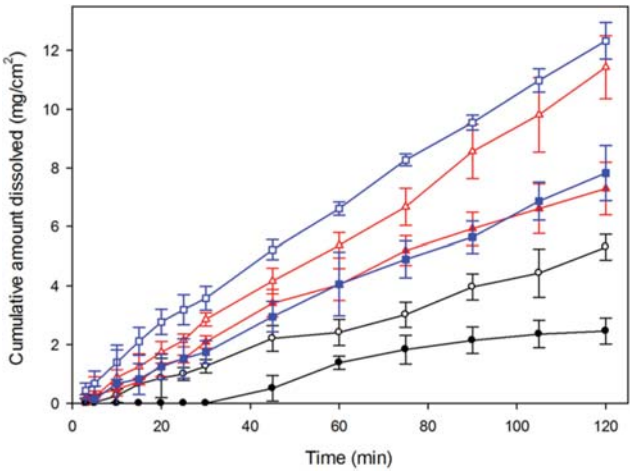

Fig. 10. Intrinsic dissolution rate (IDR) profiles of AGO (black circle), AGO-RES co-crystal (blue square), and AGO-HYQ co-crystal (red triangle) in phosphate buffer (pH 6.8, filled) and hydrochloric acid buffer (pH 1.2, empty).

Table 5. Solubility and dissolution data for AGO and its co- crystals

Solid form	Solubility (mg/mL)		IDR (mg/cm^2·min)	
	Peak position	At 24 h	pH 1.2	pH 6.8
AGO	-	0.13	0.044	0.02
AGO-RES	0.368	0.303	0.103	0.065
AGO-HYQ	0.545	0.431	0.095	0.061

files of AGO, AGO-RES, and AGO-HYQ pellets are shown in Fig. 10 and the calculated IDR values are summarized in Table 5. Similar to the observation in solubility testing, both co-crystals gave increased dissolution rates over the pure AGO. Three-fold increase in the dissolution rate was achieved in the hydrochloric acid buffer medium, whereas a two-fold enhancement was observed in the phosphate buffer solution.

It was reported that UV-Vis spectra of solutions can be employed to differentiate co-crystals from physical mixtures in solution [39]. It seems feasible to monitor the whole process of solvation during the dissolution testing for pharmaceutical co-crystals.

CONCLUSION

A screening study to prepare agomelatine (AGO) co-crystals with three dihydroxybenzene isomers, resorcinol (RES), hydroquinone (HYQ) and catechol (CAT), based on a secondary amide-hydroxyl hetero-synthon design was conducted. A novel AGO-RES co-crystal and AGO-HYQ co-crystal form I was synthesized. DSC analysis of the mixture of two co-crystal-forming components made the relationship between eutectic and co-crystal phases evident. FTIR and Raman spectroscopy made certain the existence of hydrogen bonding interactions between the amide group of AGO and the hydroxyl groups of the coformer to create co-crystal lattices, which supports the usefulness of these two spectroscopic measurement tools.

The primary motivation for investigating pharmaceutical co-crystals was to improve the aqueous solubility of insoluble drug substances. Both AGO-RES and AGO-HYQ co-crystals showed substantial enhancement in this aspect, showing a higher solubility and dissolution rates than the pure AGO. Even though HYQ is less soluble than RES in water, the AGO-HYQ co-crystal was more soluble than the AGO-RES co-crystal. This is probably due to the gradual transformation of co-crystals after dissolution, into various metastable crystalline forms of AGO, which could greatly affect the pharmaceutical behavior and effectiveness of AGO.

ACKNOWLEDGEMENTS

This research was supported by the Basic Science Research Program through the National Research Foundation of Korea funded by the Ministry of Education (NRF-2014R1A1A2056702). We also acknowledge the support of Soonchunhyang University for this research. In addition, M.-J. Lee is grateful to Dr. Srinivasulu Aitipamula (Crystallization and Particle Science, Institute of Chemical and Engineering Sciences, A*STAR) for crystal structure analysis and helpful comments on this manuscript as well.

REFERENCES

1. R. Prohens, R. Barbas, A. Portell, M. Font-Bardia, X. Alcobé and C. Puigjaner, *Cryst. Growth Des.*, **16**, 1063 (2016).
2. P. Vishweshwar, J. A. McMahon, J. A. Bis and M. J. Zaworotko, *J. Pharm. Sci.*, **95**, 499 (2006).
3. N. J. Babu and A. Nangia, *Cryst. Growth Des.*, **11**, 2662 (2011).
4. S. Aitipamula, R. Banerjee, A. K. Bansal, K. Biradha, M. L. Cheney, A. R. Choudhury, G. R. Desiraju, A. G. Dikundwar, R. Dubey, N. Duggirala, P. P. Ghogale, S. Ghosh, P. K. Goswami, N. R. Goud, R. R. K. R. Jetti, P. Karpinski, P. Kaushik, D. Kumar, V. Kumar, B. Moulton, A. Mukherjee, G. Mukherjee, A. S. Myerson, V. Puri, A. Ramanan, T. Rajamannar, C. M. Reddy, N. Rodriguez-Hornedo, R. D. Rogers, T. N. G. Row, P. Sanphui, N. Shan, G. Shete, A. Singh, C. C. Sun, J. A. Swift, R. Thaimattam, T. S. Thakur, R. K. Thaper, S. P. Thomas, S. Tothadi, V. R. Vangala, N. Variankaval, P. Vishweshwar, D. R. Weyna and M. J. Zaworotko, *Cryst. Growth Des.*, **12**, 2147 (2012).
5. US FDA, Guidance for Industry: Regulatory Classification of Pharmaceutical Co-crystals; http://www.fda.gov/downloads/Drugs/GuidanceComplianceRegulatoryInformation/Guidances/UCM516813.pdf (2016).
6. US FDA, Guidance for Industry: Regulatory Classification of Pharmaceutical Co-crystals, http://www.fda.gov/downloads/Drugs/GuidanceComplianceRegulatoryInformation/Guidances/UCM281764.pdf (2013).
7. US FDA. Generally Regarded as Safe, http://www.fda.gov/Food/IngredientsPackagingLabeling/GRAS/.
8. US FDA. Everything Added to Food Stuff in the United States, http://www.fda.gov/Food/ IngredientsPackagingLabeling/FoodAdditivesIngredients/ucm115326.htm, http://www.accessdata.fda.gov/scripts/fcn/fcnnavigation.cfm?rpt=eafuslisting.
9. J. F. Remenar, M. L. Peterson, P. W. Stephens, Z. Zhang, Y. Zimenkov and M. B. Hickey, *Mol. Pharm.*, **4**, 386 (2007).
10. A. Bak, A. Gore, E. Yanez, M. Stanton, S. Tufekcic, R. Syed, A.

Akrami, M. Rose, S. Surapaneni, T. Bostick, A. King, S. Neervannan, D. Ostovic and A. Koparkar, *J. Pharm. Sci.*, **97**, 3942 (2008).
11. M. B. Hickey, M. L. Peterson, L. A. Scoppettuolo, S. L. Morrisette, A. Vetter, H. Guzman, J. F. Remenar, Z. Zhang, M. D. Tawa, S. Haley, M. J. Zaworotko and O. Almarsson, *Eur. J. Pharm. Biopharm.*, **67**, 112 (2007).
12. N. Schultheiss and A. Newman, *Cryst. Growth Des.*, **9**, 2950 (2009).
13. M.-J. Lee, I.-C. Wang, M.-J. Kim, P. Kim, K.-H. Song, N.-H. Chun, H.-G. Park and G. J. Choi, *Korean J. Chem. Eng.*, **32**, 1910 (2015).
14. K. Demyttenaere, *Eur. Neuropsychopharmacol.*, **21**, S703 (2011).
15. C. de Bodinat, B. Guardiola-Lemaitre, E. Mocaër, P. Renard, C. Muñoz and M. J. Millan, *Nat. Rev. Drug Discov.*, **9**, 628 (2010).
16. VALDOXAN® - Product Information. http://www.guildlink.com.au/gc/ws/servier/pi.cfm?product= sepvaldx.
17. S. L. Zheng, J. M. Chen, W. X. Zhang and T. B. Lu, *Cryst. Growth Des.*, **11**, 466 (2011).
18. Q. Zhang, L. Jiang and X. Mei, *Pharm. Dev. Technol.*, **21**, 196 (2016).
19. Y. Yan, J. M. Chen, N. Geng and T. B. Lu, *Cryst. Growth Des.*, **12**, 2226 (2012).
20. H. S. Yin, Q. M. Zhang, Y. L. Zhou, Q. Ma, T. Liu, L. H. Zhu and S. Y. Ai, *Electrochim. Acta*, **56**, 2748 (2011).
21. S. Cherukuvada and A. Nangia, *Chem. Commun.*, **50**, 906 (2014).
22. J. Tata, D. Scalarone, M. Lazzari and O. Chiantore, *Euro. Polymer J.*, **45**, 2520 (2009).
23. E. Lu, N. Rodriguez-Hornedo and R. Suryanarayanan, *CrystEngComm.*, **10**, 665 (2008).
24. H. Yamashita, Y. Hirakura, M. Yuda, T. Teramura and K. Terada, *Pharm Res.*, **30**, 70 (2013).
25. H. Yamashita, Y. Hirakura, M. Yuda and K. Terada, *Pharm Res.*, **31**, 1946 (2014).
26. Z. Zhou, H. M. Chan, H. H. Y. Sung, H. H. Y. Tong and Y. Zheng, *Pharm Res.*, **33**, 1030 (2016).
27. T. Friščić and W. Jones, *Cryst. Growth Des.*, **9**, 1621 (2009).
28. K. Chadwick, R. Davey and W. Cross, *CrystEngComm.*, **9**, 732 (2007).
29. R. Tamura and M. Miyata, *Advances in organic crystal chemistry: Comprehensive reviews*, Springer Japan, Tokyo (2015).
30. R. Kaur and T. N. G. Row, *Cryst. Growth Des.*, **12**, 2744 (2012).
31. R. Kaur, S. Cherukuvada, P. B. Managutti and T. N. G. Row, *CrystEngComm.*, **18**, 3191 (2016).
32. A. Alhalaweh, S. George, A. Basavoju, S. L. Childs, S. A. A. Rizvic and S. P. Velaga, *CrystEngComm.*, **14**, 5078 (2012).
33. M. A. Elbagerma, H. G. M. Edwards, T. Munshi and I. J. Scowen, *CrystEngComm.*, **13**, 1877 (2011).
34. D. W. Mayo, F. A. Miller and R. W. Hannah, Course notes on the interpretation of infrared and Raman spectra, Wiley, New Jersey (2004).
35. G. Socrates. *Infrared and Raman characteristic group frequencies: Tables and charts*, 3rd Ed., Wiley, New York (2001).
36. D. J. Good and N. Rodriguez-Hornedo, *Cryst. Growth Des.*, **9**, 2252 (2009).
37. DrugBank - Agomelatine, https://www.drugbank.ca/drugs/DB06594.
38. W. Du, Y. Zhou, Y. Gong and C. Zhao, *Asian J. Pharm. Sci.*, **8**, 181 (2013).
39. R. Saha, S. Sengupta, S. K. Dey, I. M. Steele, A. Bhattacharyya, S. Biswas and S. Kumar, *RSC Adv.*, **4**, 49070 (2014).